NANO LETTERS

Letter

pubs.acs.org/NanoLett

Two-Dimensional Chalcogenide Nanoplates as Tunable Metamaterials via Chemical Intercalation

Judy J. Cha,[†] Kristie J. Koski,[†] Kevin C. Y. Huang,[‡] Ken Xingze Wang,[§] Weidong Luo,[∥] Desheng Kong,[†] Zongfu Yu,[‡] Shanhui Fan,[‡] Mark L. Brongersma,*[,†,∥] and Yi Cui*[,†,∥,⊥]

[†]Department of Materials Science and Engineering, [‡]Department of Electrical Engineering, [§]Department of Applied Physics, and [∥]Geballe Laboratory for Advanced Materials, Stanford University, Stanford, California 94305, United States

[⊥]Stanford Institute for Materials and Energy Sciences, SLAC National Accelerator Laboratory, 2575 Sand Hill Road, Menlo Park, California 94025, United States

Supporting Information

ABSTRACT: New plasmonic materials with tunable properties are in great need for nanophotonics and metamaterials applications. Here we present two-dimensional layered, metal chalcogenides as tunable metamaterials that feature both dielectric photonic and plasmonic modes across a wide spectral range from the infrared to ultraviolet. The anisotropic layered structure allows intercalation of organic molecules and metal atoms at the van der Waals gap of the host chalcogenide, presenting a chemical route to create heterostructures with molecular and atomic precision for photonic and plasmonic applications. This marks a departure from a lithographic method to create metamaterials. Monochromated electron energy-loss spectroscopy in a scanning transmission electron microscope was used to first establish the presence of the dielectric photonic and plasmonic modes in M_2E_3 (M = Bi, Sb; E = Se, Te) nanoplates and to observe marked changes in these modes after chemical intercalation. We show that these modal properties can also be tuned effectively by more conventional methods such as thickness control and alloy composition of the nanoplates.

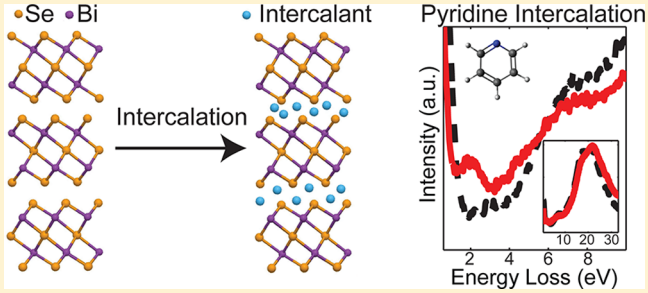

KEYWORDS: *Two-dimensional materials, chalcogenides, plasmonics, photonics, EELS*

Following the success of graphene and boron nitride, two-dimensional (2D) layered metal chalcogenides are being intensely investigated for their electrical, chemical, and optical properties.[1] Notable examples include Bi_2Se_3 and Bi_2Te_3 topological insulators for the spin-polarized, robust surface electrons[2] and MoS_2 thin films for thin-film transistors[3] and hydrogen evolution reaction.[4] The layered crystal structure provides a unique opportunity to tune the materials properties by controlling the layer thickness and by inserting guest species at the van der Waals gap, known as intercalation. Thus, novel applications in addition to currently studied spintronics, optical sensors, transistors, and catalysts may be possible. Here, we explore 2D metal chalcogenides as a potential material platform for plasmonic and photonic applications due to the combination of the precise thickness control down to a single layer and intercalation of various functional building blocks.

Because of their ability to squeeze electromagnetic energy into extremely small volumes, plasmons have enabled many novel applications including photonic chips,[5] chemical and biological sensors,[6,7] solar energy conversion,[8] photocatalysts,[9] and nanoscale lasers.[10] Noble metals such as gold and silver have been successfully used because their plasmonic responses can be effectively tuned through shape control of chemically synthesized nanoparticles, nanorods and hollow structures,[11] and the geometrical control of lithographically patterned metal structures such as holes, bowties, and metal/dielectric heterostructures.[12,13] In addition to gold and silver, there are intense interests in exploring new plasmonic materials with functionally more diverse and potentially superior properties.[14] Several materials systems include metamaterials with a gain medium,[15,16] intermetallics,[17] heavily doped semiconductors with carrier density tunability,[18,19] transparent conducting oxides,[20] and graphene.[21−23] Metamaterials in particular are hotly pursued because the optical properties of such materials can be engineered in a highly controlled fashion. Metamaterials with both metallic and semiconductor building blocks in the size range from 10 to 100 nm have been engineered to achieve unusual optical effects, such as negative refraction and cloaking.[24]

Here, we demonstrate that 2D layered chalcogenides, a historically well-known class of materials[25] that are used for thermoelectric devices as well as plasmonic applications in glass form,[26] can afford a novel chemical method to engineer the dispersion properties of plasmonic and photonic modes at molecular- and atomic-level due to the anisotropic 2D bonding

Received: August 5, 2013
Revised: November 7, 2013
Published: November 22, 2013

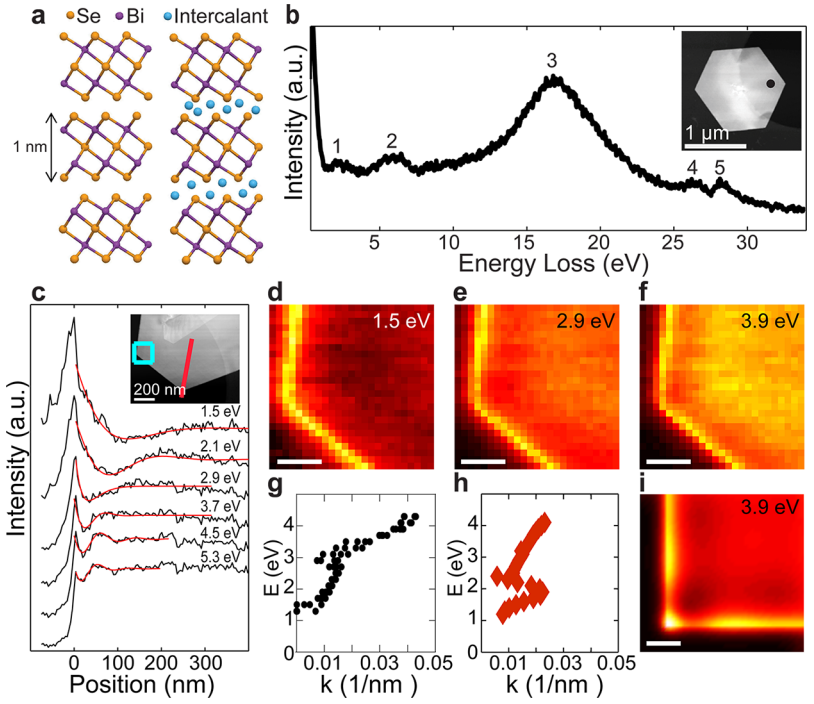

Figure 1. Photonic and plasmonic modes in Bi_2Se_3 nanoplates. (a) Crystal structure of pristine and intercalated Bi_2Se_3. (b) EELS spectrum from Bi_2Se_3 shows five peaks that are attributed to guided dielectric photonic mode (peak #1), surface plasmon (peak #2), and volume plasmon (peak #3), and Bi $O_{4,5}$ core-loss edge (peaks #4, 5). Inset shows a dark-field STEM image of a Bi_2Se_3 nanoplate. The dot denotes the location from which EELS signal is acquired. (c–g) A different nanoplate. (c) EELS line traces at specific energies along the red line, displayed with an offset for visual clarity. Red curves are exponentially decaying, sinusoidal wave fits to the measured EELS signal profiles. (d–f) The 2D maps of the photonic mode (<2.5 eV) and surface plasmons at specific energies. The maps are obtained from a 32 × 32 pixel spectral image of the plate, indicated by the blue box. Scale bars = 50 nm. Supporting Information Movie S1 plays the sequential frames of the maps. (g) Dispersion relation, obtained from the fits shown in panel d. (h) Calculated dispersion of a 10 nm thick Bi_2Se_3 dielectric slab. The dispersion trend matches the experiment. The discrepancy between the experiment (g) and calculation (h) may be due to the difference in nanoplate thicknesses as well as the fact that the first-principle calculation was carried out for bulk crystal, thus the exact amplitude of the dielectric constant may be inaccurate. (i) Calculated 2D map of the surface plasmon at 3.9 eV of a 10 nm thick Bi_2Se_3 rectangular film. A rectangular geometry was used to simplify the calculation. The intensity variations are in agreement with (f). Scale bar = 50 nm.

nature. The 2D chalcogenides are layered structures where five atomic layers (Se–Bi–Se–Bi–Se in the case of Bi_2Se_3) bond covalently to form a ∼1 nm thick quintuple layer and neighboring quintuple layers interact through weak van der Waals force (Figure 1a).[2] Synthesis of these 2D chalcogenides into nanoplates and nanoribbons has been reported.[27−29] The 2D bonding nature renders the opportunity to insert guest species into the van der Waals gap through a process known as "intercalation" (Figure 1a).[30,31] We established chemical methods to intercalate various metal atoms into the chalcogenide nanostructures at high densities.[32,33] Because the guest species can have drastically different dielectric function from the host material, intercalation affords significant control over the photonic and plasmonic modal properties, carried out at molecular- and atomic-level. Although the 2D chalcogenides we investigate in this work have loss issues, they demonstrate, as a proof of concept, intercalation as a widely applicable novel chemical route to construct metamaterials for layered materials. We used a scanning transmission electron microscope (STEM) electron energy-loss spectroscopy (EELS) to study plasmonic and photonic modes supported in 2D layered chalcogenide nanoplates of M_2E_3 (M = Bi, Sb; E = Se, Te). A STEM can not only provide structural information at the atomic-scale, it can also provide valuable information about the allowed optical modes supported by nanomaterials by enabling local EELS measurements. EELS has proven itself as a very powerful technique to study plasmon excitations in nanostructures, as shown in a recent study of surface plasmon mapping in triangular silver nanoplates[34] and quantum size effects on plasmon resonances in silver nanoparticles.[35,36] EELS can also probe dielectric photonic modes,[37] as demonstrated in STEM-EELS studies of silicon photonic crystals.[38] The ability to map optical modes in such systems is based on the fact that the EELS signal is directly proportional to the component of the local density of optical states (LDOS) along the electron beam trajectory ρ_z (typically taken as the z-direction).[39] This quantity is in turn proportional (rigorously in nondissipative systems) to the z-component of the electric field of the eigenmodes m of a nanostructure at Eigen-energies $\hbar\omega_m$

$$\rho_z(\omega, \vec{r}) \approx \sum_m |E_z(\vec{r})^m|^2 \delta(\omega - \omega_m) \quad (1)$$

By mapping the EELS signal at different energy losses, one can thus obtain maps of the optical modes supported at that energy.[39] The range of energy losses that can be captured in our monochromated EELS system is from 0.5–30 eV at the dispersion setting that gives the energy resolution of ∼0.14 eV, sufficient for this study.

Our STEM-ELLS study on chalcogenide nanoplates proceeds by first experimentally demonstrating the existence of dielectric photonic and plasmonic modes and by analyzing their dispersion relations. The presence of these two types of

dx.doi.org/10.1021/nl402937g | Nano Lett. 2013, 13, 5913−5918

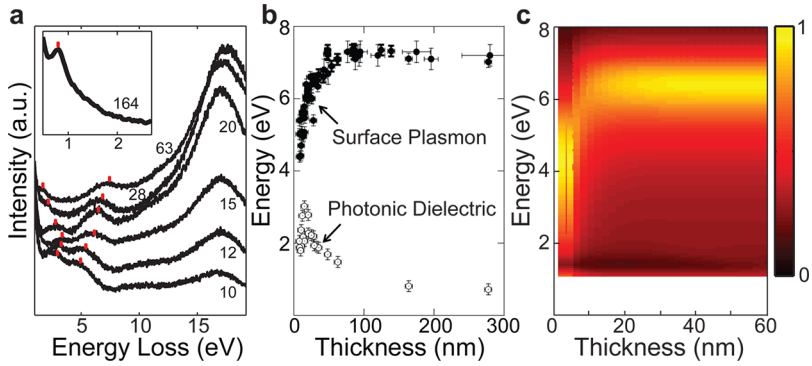

Figure 2. Thickness control over dielectric photonic and plasmonic modes in 2D chalcogenides. (a) EELS spectra from Bi_2Se_3 plates of different thicknesses show systematic shifts in the dielectric photonic and surface plasmon peaks, showing the ability to engineer dispersion in these nanomaterials by controlling the thickness. Numbers indicate plate thicknesses in nanometers. The red dots are a visual guide. For clarity, the EELS spectrum for a 164 nm thick ribbon is displayed separately as inset. (b) Peak energies plotted against the plate thickness. (c) Calculated EELS signal resulting from surface plasmon excitations as a function of the plate thickness. The color represents intensity where yellow denotes higher intensity, as indicated in the color scale.

modes is consistent with first-principle calculations of the dielectric function of these materials. Supporting Information Figure S1 shows a representative calculation for the specific case of Bi_2Se_3. The real part of its dielectric constant is large and positive in the visible and infrared part of the spectrum, where it can support dielectric photonic modes, and negative at higher energies in the ultraviolet where it supports plasmons.[40] We then continue by showing how the dispersive properties of the photonic and plasmonic modes can be engineered by the more-or-less established means of tuning the plate thickness and composition. Finally, we demonstrate the new tantalizing opportunity to atomically engineer these modes by means of chemical intercalation.

A monochromated EELS spectrum taken from a Bi_2Se_3 nanoplate shows five distinct peaks (labeled from 1 to 5, Figure 1b). Consistent with the spectral features of the dielectric function of Bi_2Se_3 (Supporting Information Figure S1), the lowest energy loss peak is assigned to a dielectric photonic guided mode, while the peak at 6.4 eV is attributed to surface plasmon excitation. The third peak at ~17 eV is a volume plasmon, and the remaining two peaks at even higher energies are core-loss Bi 5d electron transitions ($O_{4,5}$ edge).[41] To further confirm these assignments, we use EELS to obtain their dispersion relation and make a comparison to theory. To this end we map the spatial properties of the modes near the edge of a ~ 16 nm thick nanoplate. Figure 1d–f (and also Supporting Information Figures S2 and S3) shows EELS maps taken at different loss energies (1.5, 2.9, and 3.9 eV) over an integration window of 0.3 eV. Each map exhibits a spatial variation of the EELS signal with a characteristic dark band close to the edge of the plate. The width of this band depends on the magnitude of the energy loss (Supporting Information Movies S1 and S2 play sequential frames of EELS maps that clearly show gradual reduction of the dark band with increasing energy loss). A calculated surface plasmon intensity map at 3.9 eV of a 10 nm thick Bi_2Se_3 rectangular film shows similar intensity variations (Figure 1i). The spatial variation of the EELS signal near the plate edge can be explained with an intuitive classical picture, where the electric fields induced by the electron beam in the plate act back on the electron in a spatially dependent fashion. For example, at some spatial locations an incident electron can excite a guided wave in the plate, which after reflection of the plate edge can act back on the next incoming electron to slow it down, that is, to induce energy loss. Thus, the surface plasmon is actually the surface plasmon polariton. When propagating modes are excited, eq 1 predicts that the spatial variations in the EELS signal at a certain energy loss will occur with a characteristic spatial frequency that is twice the spatial frequency of the relevant mode, that is, $2k_m$. This is because EELS measures intensity, not the field amplitude. Figure 1c shows characteristic EELS signal traces taken along the red line (inset) at different energies in the range from 1. 5 to 5.3 eV. By fitting these traces with exponentially decaying sine waves one can obtain an approximate dispersion relationship for the supported modes as shown in Figure 1g. Figure 1h shows the simulated dispersion relations for the dielectric photonic and plasmonic modes as obtained by using the fitted materials dispersion as given in Supporting Information Figure S1. The experimental and simulated curves exhibit similar qualitative trends for the dielectric photonic and plasmonic modes, further confirming our mode assignment. Quantitative differences can be expected based on the inaccuracy in the presented calculation of the dielectric constant, but are within reasonable bounds (Supporting Information Figure S1). The photonic and plasmonic maps (Figure 1) suggest that Bi_2Se_3 is lossy as the modal propagation extends to a few hundred nanometers only. This can be deduced from the high imaginary part of the dielectric function between 2 and 3.5 eV energy range (Supporting Information Figure S1).

Next, we explore the possibility to geometrically tune the modal dispersion of the dielectric photonic and plasmonic modes. The 2D nature of layered chalcogenides naturally allows for precise control over layer thickness. Extremely thin films down to a single quintuple layer were found to be stable.[42] Figure 2a,b shows the impact of the plate thickness in the range from 10 − 300 nm on the modal dispersion (Supporting Information Figure S4 explains the thickness calibration). With decreasing thickness from 300 to 10 nm, the dielectric photonic peak in the EELS spectrum shifts to higher energies from 0.7 to ~3 eV while the surface plasmon peak shifts to lower energies from 7.1 to 4.5 eV. Bi_2Se_3 nanoplates are the dielectric waveguide that carries the photonic mode and the modal energy of the photonic mode is dictated by the thickness of the plate. The lateral dimensions of the plates are much larger than the thickness and thus do not affect the modal energy. The blue

dx.doi.org/10.1021/nl402937g | Nano Lett. 2013, 13, 5913−5918

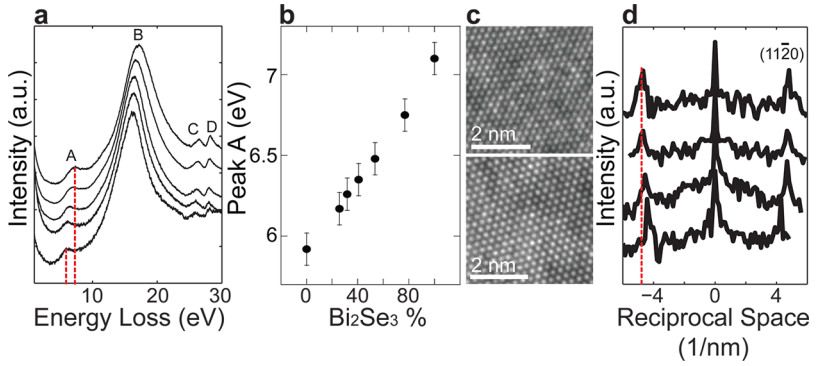

Figure 3. Plasmon tuning via compositional control of $Bi_2(Se_xTe_{1-x})_3$ nanoribbons. (a) EELS spectra taken from $Bi_2(Se_xTe_{1-x})_3$ nanoribbons with different values of x. From bottom to top, x are 0, 0.26, 0.41, 0.77, and 1, respectively. Shifts in plasmon peaks due to compositional changes are clear. (b) Peak A position, plotted against the percentage of Bi_2Se_3 in $Bi_2(Se_xTe_{1-x})_3$. (c) High-resolution TEM images of Bi_2Se_3 (top) and Bi_2Te_3 (bottom) nanoribbons, showing larger lattice constants for Bi_2Te_3. (d) Intensity profiles of diffractograms, Fourier transform of lattice images, of $Bi_2(Se_xTe_{1-x})_3$ nanoribbons with different values of x. From bottom to top, x are 0, 0.42, 0.77, and 1, respectively. The lattice spacing decreases systematically with increasing x.

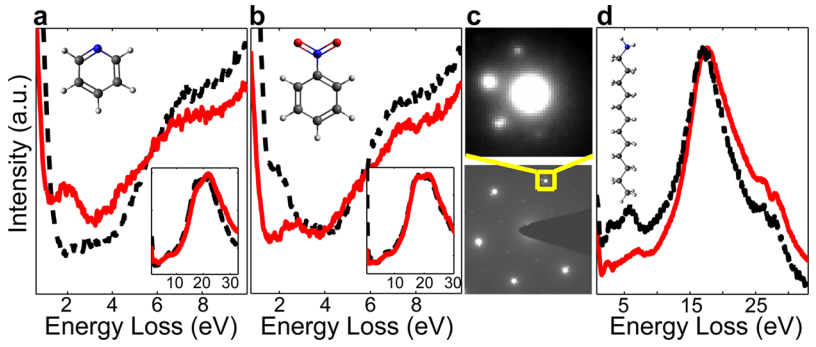

Figure 4. Pyridine-, nitrobenzene-, and dodecylamine-intercalated Bi_2Se_3 and corresponding changes in EELS spectra. (a) EELS signal before (dotted black) and after (solid red) pyridine intercalation. The presence of the photonic mode is apparent after intercalation. Inset shows a pyridine molecule. (b) EELS signal before (dotted black) and after (solid red) nitrobenzene intercalation. The EELS signal for the photonic mode at ~2 eV decreases distinctly after intercalation. Inset shows a nitrobenzene molecule. (c) Electron diffraction of a dodecylamine-intercalated Bi_2Se_3 ribbon, showing incommensurate charge density wave formation due to intercalation. (d) EELS signal of a clean Bi_2Se_3 nanoribbon (dotted black) and a dodecylamine-intercalated Bi_2Se_3 nanoribbon (slid red). The spectral shape has distinctly altered from pristine Bi_2Se_3. The inset shows a dodecylamine molecule.

shift of the photonic peak is explained by the fact that the dispersion relation for dielectric slab modes shifts up for thinner slabs due to the increased modal overlap with the lower index surroundings (vacuum). In the meantime, the red shift of the surface plasmon mode is due to enhanced surface plasmon coupling between the top and bottom surfaces in thinner plates which pushes the entire surface plasmon dispersion curve to lower energies.[43] These results directly show the ability to tune modal dispersion by thickness control and provide further evidence that our initial modal assignment is correct. As expected, the volume plasmon does not change with thickness. Finite-difference time-domain (FDTD) calculations of the surface plasmon of Bi_2Se_3 slabs (Figure 2c) show good agreement with the experiment. EELS loss functions including full retardation effects are also calculated for different slab thicknesses and show the same result (Supporting Information Figure S5).

The presence of the observed photonic and plasmonic modes turns out to be a general property for a family of binary chalcogenides, including Bi_2Se_3, Bi_2Te_3 and Sb_2Te_3, paving the way for compositional control over the modal properties. As the "parent" compounds share the same crystal structure, we can grow ternary chalcogenides $Bi_2(Se_xTe_{1-x})_3$ and $(Sb_xBi_{1-x})_2Te_3$ with arbitrary composition,[44,45] which affords an opportunity to tune the property by alloying at the atomic scale. As the ratio x changes from 0 to 1 in $Bi_2(Se_xTe_{1-x})_3$, lattice constant and dielectric permittivity should change from those of Bi_2Te_3 to Bi_2Se_3. To eliminate surface plasmon coupling effects due to thickness changes, EELS spectra in this part of the study are measured from thick $Bi_2(Se_xTe_{1-x})_3$ nanoribbons. All plasmon peaks shift systematically with the ratio x (Figure 3a,b), for example, from 5.9 eV at x = 0 to 7.1 eV at x = 1 for peak A. Interestingly, the peak energy has a linear dependence on composition x, which makes precise control possible. We note that no subtraction procedures such as subtracting the tail intensity of the zero loss peak or subtracting the intensity contribution from the volume plasmon were carried out in determining the peak position of the surface plasmon. High-resolution TEM images show larger lattice spacing for Bi_2Te_3, compared to Bi_2Se_3 (Figure 3c), and correspondingly Bi_2Te_3 plasmons are at lower energies than Bi_2Se_3 plasmons. The gradual change in the lattice constant of $Bi_2(Se_xTe_{1-x})_3$ with increasing x is revealed by the systematic shift of the (11$\bar{2}$0) diffraction peak, obtained by Fourier transform of high-resolution TEM images (Figure 3d). The atomic ratio x is measured by TEM-energy dispersive X-ray spectroscopy. Plasmons of thick $(Sb_xBi_{1-x})_2Te_3$ nanoplates also show systematic shifts (Supporting Information Figure S6). We

dx.doi.org/10.1021/nl402937g | Nano Lett. 2013, 13, 5913−5918

note that the charge carrier type and density also depend on the composition in these ternary chalcogenides,[44,45] offering a platform of plasmonic materials with rich electrical and optical properties.

Owing to the chalcogenides' 2D nature, intercalation can be used as a completely new way to tune the photonic and plasmonic modes by making heterostructures of chalcogenide and intercalant layers at molecular and atomic scale. It is well documented that various organic molecules and alkali metals can readily be intercalated into the van der Waals gap of these layered chalcogenides.[32,33,46] High densities of pyridine have been intercalated into the van der Waals gaps of TaS_2,[47] and recently up to 60% of Cu atoms were intercalated into Bi_2Se_3 nanoribbons.[32] These intercalants can change the dielectric permittivity of Bi_2Se_3 significantly, thus presenting intercalated Bi_2Se_3 as new plasmonic metamaterials. We compared EELS spectra of Bi_2Se_3 nanoplates before and after pyridine (C_5H_5N) and nitrobenzene ($C_6H_5NO_2$) intercalation and also examined dodecylamine ($C_{12}H_{27}N$)-intercalated Bi_2Se_3 nanoribbons. Intercalation was carried out by placing SiN_x TEM grids that contained examined Bi_2Se_3 nanoplates in intercalant solution for 26 h under reflux; excess solution was washed off with ethanol or acetone.

The morphology of the nanoplates is found to be intact after intercalation, and the electron diffraction pattern shows a redistribution of the intensities among diffraction peaks. For dodecylamine intercalation, incommensurate charge density waves are sometimes observed in the diffraction pattern confirming successful intercalation (Figure 4c).[48] After intercalation, the photonic mode is enhanced visibly in pyridine-intercalated Bi_2Se_3 (Figure 4a) while it is reduced in nitrobenzene-intercalated Bi_2Se_3 (Figure 4b). Multiple plates consistently show such results for both intercalations (Supporting Information Figures S7 and S8). For dodecylamine intercalation, direct comparison before and after intercalation was difficult because residual solution could not be completely removed. Thus, we compare dodecylamine-intercalated Bi_2Se_3 ribbons with pristine ribbons. The optical mode at ~2 eV appears much enhanced in dodecylamine-intercalated Bi_2Se_3 and the plasmon mode becomes asymmetrical (Figure 4d). We tentatively attribute the enhancement of the photonic mode to a reduction of the imaginary part of the dielectric permittivity for pyridine and dodecylamine intercalation. The DC dielectric constants of pyridine and dodecylamine are ~12 and ~5, respectively, while that of nitrobenzene is ~35.[49] The marked difference in the dielectric constants of pyridine versus nitrobenzene is due to the different dipole moments in these molecules; the dipole moment of nitrobenzene (3.98 D) is almost twice as large as that of pyridine (2.2 D).[50] This leads to a wide tunability of the photonic property of the host material using organic molecules of similar sizes and structures and yet with very different dielectric constants. We note that additional changes in the electronic band structure may be induced by intercalation, which may contribute to the observed changes in the EELS spectra. Because of the limited tilt range in the electron microscope, anisotropic excitation of photonic modes possibly due to intercalation could not be carefully investigated. In addition to organic molecules, copper-intercalated Bi_2Se_3 also show distinct plasmon responses (Supporting Information Figure S9) although detailed study is left for future.

In summary, we demonstrated the presence of dielectric photonic and plasmonic modes in thin 2D chalcogenides nanoplates. We presented three distinct ways to tune the dispersion of these modes via thickness and composition control as well as chemical intercalation of organic molecules and metals in the van der Waals gap. Intercalation, in particular, presents an exciting opportunity for emergence of new fundamental phenomena and potential optoelectronic applications. Anticipated functionality or applications of atomic-scale metamaterials achieved via intercalation may be quantum plasmonic effects where the intercalated metal sheets are separated by a single chalcogenide layer or indefinite metamaterials. The combination of thickness control, compositional tuning, and intercalation chemistry in 2D chalcogenide nanoplates paves a way for the development of new plasmonic and photonic metamaterials that can be engineered at multiple length scales simultaneously. One issue with the chalcogenide nanoplates studied here is the relatively high loss, which must be overcome for wide applications. Intercalating gain medium may be one solution. This work also highlights the ability of a transmission electron microscope to study and correlate optical phenomena in nanomaterials to their structural properties at a length scale well below the diffraction limit.

■ ASSOCIATED CONTENT

Ⓢ Supporting Information

Methods including materials synthesis, intercalation, experimental setup, and simulation details. Additional figures and supporting movies. This material is available free of charge via the Internet at http://pubs.acs.org.

■ AUTHOR INFORMATION

Corresponding Authors

*E-mail: (Y.C.) yicui@stanford.edu.
*E-mail: (M.B.) brongersma@stanford.edu.

Author Contributions

The manuscript was written through contributions of all authors. All authors have given approval to the final version of the manuscript.

Notes

The authors declare no competing financial interest.

■ ACKNOWLEDGMENTS

Y.C. acknowledges support by the Department of Energy, Office of Basic Energy Sciences, Materials Sciences and Engineering Division, under contract DE-AC02-76-SFO0515. K.H and M.L.B acknowledge support from a Multidisciplinary University Research Initiative from the Air Force Office of Scientific Research (AFOSR MURI Award No. FA9550-12-1-0488). Authors thank Ai Leen Koh for her help in initial EELS experiments.

■ REFERENCES

(1) Butler, S. Z.; et al. *ACS Nano* **2013**, *7*, 2898−2926.
(2) Zhang, H.; Liu, C.-X.; Qi, X.-L.; Dai, X.; Fang, Z.; Zhang, S.-C. *Nat. Phys.* **2009**, *5*, 438−442.
(3) Radisavljevic, B.; Radenovic, A.; Brivio, J.; Giacometti, V.; Kis, A. *Nat. Nanotechnol.* **2010**, *6*, 147−150.
(4) Jaramillo, T. F.; Jørgensen, K. P.; Bonde, J.; Nielsen, J. H.; Horch, S.; Chorkendorff, I. *Science* **2007**, *317*, 100−102.
(5) Ozbay, E. *Science* **2006**, *311*, 189−193.
(6) Nie, S.; Emory, S. R. *Science* **1997**, *275*, 1102−1106.
(7) Sonnichsen, C.; Reinhard, B. M.; Liphardt, J.; Alivisatos, A. P. *Nat. Biotechnol.* **2005**, *23*, 741−745.
(8) Atwater, H. A.; Polman, A. *Nat. Mater.* **2010**, *9*, 205−213.

(9) Linic, S.; Christopher, P.; Ingram, D. B. *Nat. Mater.* **2011**, *10*, 911−921.
(10) Hill, M. T.; et al. *Nat. Photonics* **2007**, *1*, 589−594.
(11) Link, S.; El-Sayed, M. A. *J. Phys. Chem. B* **1999**, *103*, 4212−4217.
(12) Ebbesen, T. W.; Lezec, H. J.; Ghaemi, H. F.; Thio, T.; Wolff, P. A. *Nature* **1998**, *391*, 667−669.
(13) Fang, N.; Lee, H.; Sun, C.; Zhang, X. *Science* **2005**, *308*, 534−537.
(14) Boltasseva, A.; Atwater, H. A. *Science* **2011**, *331*, 290−291.
(15) Hess, O.; Pendry, J. B.; Maier, S. A.; Oulton, R. F.; Hamm, J. M.; Tsakmakidis, K. L. *Nat. Mater.* **2012**, *11*, 573−584.
(16) Xiao, S.; Drachev, V. P.; Kildishev, A. V.; Ni, X.; Chettiar, U. K.; Yuan, H.-K.; Shalaev, V. M. *Nature* **2010**, *466*, 735−738.
(17) Blaber, M. G.; Arnold, M. D.; Ford, M. J. *J. Phys.: Condens. Matter* **2009**, *21*, 144211.
(18) Naik, G. V.; Boltasseva, A. *Phys. Status Solidi RRL* **2010**, *4*, 295−297.
(19) Luther, J. M.; Jain, P. K.; Ewers, T.; Alivisatos, A. P. *Nat. Mater.* **2011**, *10*, 361−366.
(20) West, P. R.; Ishii, S.; Naik, G. V.; Emani, N. K.; Shalaev, V. M.; Boltasseva, A. *Laser Photonics Rev.* **2010**, *4*, 795−808.
(21) Jablan, M.; Buljan, H.; Soljačić, M. *Phys. Rev. B* **2009**, *80*, 245435.
(22) Chen, J.; et al. *Nature* **2012**, *487*, 77−81.
(23) Fei, Z.; et al. *Nature* **2012**, *487*, 82−85.
(24) Shalaev, V. M. *Nat. Photonics* **2007**, *1*, 41−48.
(25) Devillanova, F. A. *Handbook of Chalcogen Chemistry: New Perspectives in Sulfur, Selenium and Tellurium*; RSC Pub: Cambridge, 2007.
(26) Sámson, Z. L.; Yen, S.-C.; MacDonald, K. F.; Knight, K.; Li, S.; Hewak, D. W.; Tsai, D.-P.; Zheludev, N. I. *Phys. Status Solidi RRL* **2010**, *4*, 274−276.
(27) Peng, H.; Lai, K.; Kong, D.; Meister, S.; Chen, Y.; Qi, X.-L.; Zhang, S.-C.; Shen, Z.-X.; Cui, Y. *Nat. Mater.* **2010**, *9*, 225−229.
(28) Kong, D.; Dang, W.; Cha, J. J.; Li, H.; Meister, S.; Peng, H.; Liu, Z.; Cui, Y. *Nano Lett.* **2010**, *10*, 2245−2250.
(29) Kong, D.; Randel, J. C.; Peng, H.; Cha, J. J.; Meister, S.; Lai, K.; Chen, Y. L.; Sheng, Z. X.; Manoharan, H. C.; Cui, Y. *Nano Lett.* **2010**, *10*, 329−333.
(30) Whittingham, M. S.; Jacobson, A. J. *Intercalation chemistry*; Whittingham, M. S. , Jacobson, A. J., Eds.; Academic Press: New York, 1982.
(31) Dresselhaus, M. S. *Intercalation in layered materials*; Dresselhaus, M. S., Ed.; Plenum Press: New York, 1986.
(32) Koski, K. J.; Cha, J. J.; Reed, B. W.; Wessells, C. D.; Kong, D.; Cui, Y. *J. Am. Chem. Soc.* **2012**, *134*, 7584−7587.
(33) Koski, K. J.; Wessells, C. D.; Reed, B. W.; Cha, J. J.; Kong, D.; Cui, Y. *J. Am. Chem. Soc.* **2012**, *134*, 13773.
(34) Nelayah, J.; et al. *Nat. Phys.* **2007**, *3*, 348−353.
(35) Ouyang, F.; Batson, P. E.; Isaacson, M. *Phys. Rev. B* **1992**, *46*, 15421−15425.
(36) Scholl, J. A.; Koh, A. L; Dionne, J. A. *Nature* **2012**, *483*, 421−427.
(37) Garcia de Abajo, F. J.; Kociak, M. *Phys. Rev. Lett.* **2008**, *100*, 106804−106804.
(38) Cha, J. J.; Yu, Z.; Smith, E.; Couillard, M.; Fan, S.; Muller, D. A. *Phys. Rev. B* **2010**, *81*, 113102.
(39) Garcia de Abajo, F. J. *Rev. Mod. Phys.* **2010**, *82*, 209−275.
(40) Köhler, H.; Becker, C. R. *Phys. Status Solidi b* **1974**, *61*, 533−537.
(41) Nascimento, V. B.; de Carvalho, V. E.; Paniago, R.; Soares, E. A.; Ladeira, L. O.; Pfannes, H. D. *J. Electron Spectrosc. Relat. Phenom.* **1999**, *104*, 99−107.
(42) Coleman, J. N.; et al. *Science* **2011**, *331*, 568−571.
(43) Burke, J. J.; Stegeman, G. I.; Tamir, T. *Phys. Rev. B* **1986**, *33*, 5186−5201.
(44) Cha, J. J.; Kong, D.; Hong, S. S.; Analytis, J. G.; Lai, K.; Cui, Y. *Nano Lett.* **2012**, *12*, 1107−1111.
(45) Kong, D.; et al. *Nat. Nanotechnol.* **2011**, *6*, 705−709.
(46) Friend, R. H.; Yoffe, A. D. *Adv. Phys.* **1987**, *36*, 1−94.
(47) Parry, G. S.; Scruby, C. B.; Williams, P. M. *Philos. Mag.* **1973**, *29*, 601−612.
(48) Chen, C. H.; Gibson, J. M.; Fleming, R. M. *Phys. Rev. Lett.* **1981**, *47*, 723−725.
(49) Wohlfahrt, C. *1 Introductrion*; Madelung, O., Ed.; Spring-erMaterials - The Landolt-Bornstein Dabase, 1991.
(50) *CRC Handbook of Chemistry and Physics*, 93rd ed.; Taylor & Francis: New York, 2012.